

Effects of Coupled Dark Energy on the Milky Way and its Satellites

Camilla Penzo^{1,2*}, Andrea V. Macciò¹, Marco Baldi^{3,4,5}, Luciano Casarini⁶, Jose Oñorbe¹

¹ *Max-Planck-Institut für Astronomie, Königstuhl 17, 69117 Heidelberg, Germany;*

² *Fellow of the International Max Planck Research School for Astronomy and Cosmic Physics at the University of Heidelberg;*

³ *Dipartimento di Astronomia, Università di Bologna, Italy;*

⁴ *INAF - Osservatorio Astronomico di Bologna, via Ranzani 1, I-40127 Bologna, Italy;*

⁵ *INFN - Sezione di Bologna, viale Berti Pichat 6/2, I-40127 Bologna, Italy;*

⁶ *Departamento de Física, Universidade Federal do Espírito Santo, Av. Fernando Ferrari 514, 29075-910 Vitória (ES), Brazil*

29 April 2015

ABSTRACT

We present the first numerical simulations in coupled dark energy cosmologies with high enough resolution to investigate the effects of the coupling on galactic and sub-galactic scales. We choose two constant couplings and a time-varying coupling function and we run simulations of three Milky-Way-size halos ($\sim 10^{12} M_{\odot}$), a lower mass halo ($6 \times 10^{11} M_{\odot}$) and a dwarf galaxy halo ($5 \times 10^9 M_{\odot}$). We resolve each halo with several millions dark matter particles. On all scales the coupling causes lower halo concentrations and a reduced number of substructures with respect to Λ CDM. We show that the reduced concentrations are not due to different formation times, but they are related to the extra terms that appear in the equations describing the gravitational dynamics. On the scale of the Milky Way satellites, we show that the lower concentrations can help in reconciling observed and simulated rotation curves, but the coupling values necessary to have a significant difference from Λ CDM are outside the current observational constraints. On the other hand, if other modifications to the standard model allowing a higher coupling (e.g. massive neutrinos) are considered, coupled dark energy can become an interesting scenario to alleviate the small-scale issues of the Λ CDM model.

Key words: cosmology: dark energy, dark matter – galaxies: haloes, formation, evolution – methods: numerical

1 INTRODUCTION

Since the discovery of the accelerated expansion of the universe (Riess et al. 1998; Perlmutter et al. 1999), a Cosmological Constant Λ has been the most widely accepted explanation for the required negative pressure. Together with cold dark matter, today the dark sector is accounting for about 95% of the total energy density (Planck Collaboration et al. 2015) and builds the foundations for the so-called Λ Cold Dark Matter (Λ CDM) model.

Despite the highly successful inflationary Λ CDM paradigm, the fundamental problems associated with the introduction of a cosmological constant, namely *fine-tuning* and *coincidence* problems (Weinberg 1989), have served as

motivations for alternative descriptions of the dark sector. Introducing a time evolving scalar field (dark energy) responsible for the negative pressure is the approach of quintessence models (Wetterich 1988; Peebles & Ratra 1988) and has been one of the most popular generalizations for the cosmological constant in the last decade. Furthermore, given the currently still unknown nature of the dark sector, the possibility of a non-null coupling between dark matter and dark energy has been considered (Wetterich 1995; Anderson & Carroll 1998; Amendola 2000; Billyard & Coley 2000; Zimdahl et al. 2001; Amendola & Tocchini-Valentini 2001; Farrar & Peebles 2004; Gromov et al. 2004). Given that in these models dark matter and dark energy density evolutions are strongly coupled, this would in turn alleviate the *coincidence* problem (Mangano et al. 2003; Matarrese et al. 2003). The effects of such interaction might be seen

* penzo@mpia.de

on the Cosmic Microwave Background (CMB), on supernovae and on the growth of structures, as pointed out by Matarrese et al. (2003); Amendola (2004); Amendola et al. (2004); Koivisto (2005); Guo et al. (2007) and many others. Structure formation has been as well investigated via numerical simulations by Macciò et al. (2004); Baldi et al. (2010); Li & Barrow (2011); Carlesi et al. (2014) and their follow up works, where the statistical distribution of structures has been studied. Both Baldi et al. (2010) and Carlesi et al. (2014) found that, when introducing a coupling between dark energy and dark matter, halo concentrations decrease.

In this work, we run the first high resolution simulations on galactic scales in coupled dark energy cosmology. Our aim is to obtain high enough resolutions to investigate the properties of the dark matter distribution at sub-galactic scales, mass scales at which the effects of the coupling have not yet been studied. The subhalos that we are interested in will in turn be the hosts of dwarf galaxies and their properties can be compared with observations of satellite dwarf galaxies of both Milky Way and Andromeda. In fact, despite Λ CDM predictions on large scales being in very good agreement with galaxy clustering surveys (Jones et al. 2009; Alam et al. 2015), on galactic scales challenges between Λ CDM predictions and observations have appeared.

Firstly, the *missing satellites* problem, i.e. overabundance of substructures in Λ CDM Milky-Way size halo simulations when compared to observations of the Milky Way dwarf galaxies (Klypin et al. 1999; Moore et al. 1999). On the other hand, as showed in Madau et al. (2008) and Macciò et al. (2010), accounting for the baryonic physics drastically reduces the number of visible satellites. Secondly, the *core/cusp* problem, namely the inconsistency between the constant density cores estimated from observations and the cuspy inner density profiles found in Λ CDM simulations. See Flores & Primack (1994); Moore (1994); Diemand et al. (2005); Gentile et al. (2009); Walker & Peñarrubia (2011); Agnello & Evans (2012); Salucci et al. (2012), but also van den Bosch & Swaters (2001); Swaters et al. (2003); Simon et al. (2005). While this inconsistency can be attributed to baryonic feedback processes (e.g. Governato et al. 2012; Di Cintio et al. 2014; Oñorbe et al. 2015), for the case of Milky Way satellites the baryonic explanation is not straightforward since these objects can be almost completely dark matter dominated. Baldi et al. (2010) and Carlesi et al. (2014) showed that for halos with $M \gtrsim 10^{13} M_\odot$ the coupling between dark matter and dark energy produces density profiles that are less cuspy in the inner density regions, which can help alleviating the core/cusp problem. The aim of this work is to investigate whether this effect persists at much lower masses. Moreover, concentrations of the most massive subhalos orbiting around a Λ CDM Milky-Way size halo seem to be too high to be hosting the brightest dwarf galaxies observed. This translates into a prediction from Λ CDM numerical simulations for the existence of massive dark matter subhalos that seem to have failed at forming stars, and is known as the *too big to fail* problem (Boylan-Kolchin et al. 2011; Lovell et al. 2012; Rashkov et al. 2012; Tollerud et al. 2012).

Whether these issues bring serious challenges for the Λ CDM model or whether they can entirely be treated by invoking baryonic physics is currently under debate. With

this work we aim at studying the properties of halos and their sub-structures to determine whether coupled dark energy cosmologies can alleviate the aforementioned issues. In Section 2 we summarize the theoretical model behind coupled dark energy and we specify our choices of coupling functions. In Section 3 we described the numerical methods used to produce initial conditions and the N-body codes to run the simulations. In Section 4 we show our simulations results, for both halos and subhalos. Finally, in Section 5 we present our conclusions.

2 COSMOLOGICAL MODELS

We present a study focused on understanding the non-linear effects of coupled dark energy models on galactic scales. The models that we consider allow for an interaction between dark matter and dark energy (Amendola 2000; Billyard & Coley 2000; Zimdahl et al. 2001; Gromov et al. 2004; Macciò et al. 2004; Baldi et al. 2010) and obey the following Lagrangian:

$$\mathcal{L} = \frac{1}{16\pi G} R - \frac{1}{2} \partial^\mu \phi \partial_\mu \phi - V(\phi) - m(\phi) \bar{\psi} \psi + \mathcal{L}_{kin}[\psi], \quad (1)$$

where the mass $m(\phi)$ of the dark matter field ψ is a function of the dark energy scalar field ϕ , and the $\mathcal{L}_{kin}[\psi]$ term includes the kinetic part of the dark matter Lagrangian. The choice of $m(\phi)$ specifies the coupling and in our work we use:

$$m(\phi) = m_0 e^{-\beta(\phi) \frac{\phi}{M_{Pl}}}, \quad (2)$$

where m_0 is the mass at $z = 0$, $M_{Pl} \equiv 1/\sqrt{8\pi G}$ is the Planck mass, with G being the Newton's constant, and $\beta(\phi)$ is the coupling function. The respective continuity equations for cold dark matter and dark energy are:

$$\begin{aligned} \dot{\rho}_c + 3H\rho_c &= -\beta(\phi)\dot{\phi}\rho_c, \\ \dot{\rho}_\phi + 3H\rho_\phi &= +\beta(\phi)\dot{\phi}\rho_c, \end{aligned} \quad (3)$$

where ρ_c is the cold dark matter density and ρ_ϕ is the dark energy density, which is $\rho_\phi \equiv \dot{\phi}^2 + V(\phi)$, and $H \equiv \dot{a}/a$ is the Hubble parameter. Our choice for the self-interacting dark energy potential is $V(\phi) \propto e^{-\alpha\phi}$, with $\alpha = 0.08$.

The evolution of cold dark matter density perturbations is regulated by the following equation:

$$\ddot{\delta}_c + (2H - \beta\dot{\phi})\dot{\delta}_c - \frac{3}{2}H^2 [(1 + 2\beta^2)\Omega_c\delta_c + \Omega_b\delta_b] = 0, \quad (4)$$

where Ω_c and Ω_b are respectively the density parameters $\Omega_i \equiv \rho_i/\rho_{crit}$ for cold dark matter and baryons, and $\rho_{crit} = 8\pi G/3H^2$. Two extra terms appear in Eq. 4 compared to the Λ CDM case: a friction term $-\beta\dot{\phi}\delta_c$ and the factor $(1 + 2\beta^2)$ responsible for the enhancement of the gravitational force acting on cold dark matter particles, which is known as “fifth force”. As pointed out in Baldi (2011), in the linear regime both these extra terms produce an acceleration of growth of cold dark matter density perturbations. On the other hand, when considering the non-linear effects, the friction term is responsible for lowering the concentration of dark matter halos.

The appearance of extra terms becomes clear when calculating the acceleration felt by the i -th dark matter particle

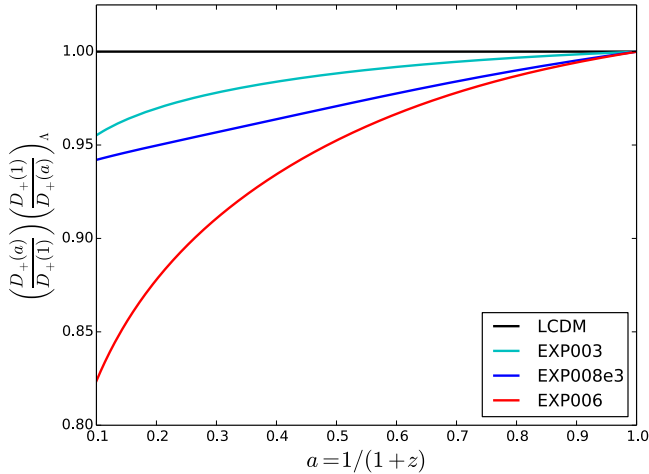


Figure 1. Linear growth factor evolutions for all cosmologies normalized to today's values divided by the Λ CDM evolution.

in a coupled dark energy cosmology for the limit of a light scalar field (see Baldi et al. 2010 for calculation):

$$\ddot{v}_i = \beta(\phi)\dot{\phi}\dot{v}_i + G[1 + 2\beta(\phi)^2] \sum_{j \neq i} \frac{m_j \vec{r}_{ij}}{|\vec{r}_{ij}|^3}. \quad (5)$$

The term $\beta(\phi)\dot{\phi}\dot{v}_i$ accelerates dark matter particles in the direction of their motion and thus lowers halo concentrations.

Based on Baldi et al. (2010) and Baldi (2011), we chose three coupling scenarios. EXP003 and EXP008e3 are observationally viable models (see Pettorino et al. 2012 for CMB constraints on the coupling value), respectively with a constant coupling $\beta = 0.15$ and a coupling $\beta(\phi)$ varying with redshift (for more details on these models we refer to Baldi 2012). We also explore an extreme constant coupling case EXP006 with $\beta = 0.3$ (about 6σ outside present observational limits, Pettorino et al. 2012) to better understand its implications.

3 NUMERICAL METHODS

3.1 Initial Conditions and Coupled Dark Energy

As in Penzo et al. (2014), we used GRAFIC-DE, an extension of the initial condition generator GRAFIC-2 (Bertschinger 2001) such that initial conditions for a generic cosmological model can be produced once the evolution of the cosmological parameters are given as an input. GRAFIC-DE requires transfer functions, evolution of the density parameters Ω_i , linear growth factor D_+ and f_Ω , the logarithmic derivative of the growth factor with respect to the scale factor. As the original code, GRAFIC-DE is able to generate multi mass initial conditions from a cosmological box. In Fig. 1 we show the evolution of the linear growth factor D_+ for all four cosmological models. The transfer functions for Λ CDM have been produced using CAMB (Lewis & Bridle 2002), while the transfer functions for the coupled dark energy models have been produced by weighting the Λ CDM transfer functions with the D_+ of the coupled model. All initial conditions were created using the same random seeds, in order to be able to identify structures among the models.

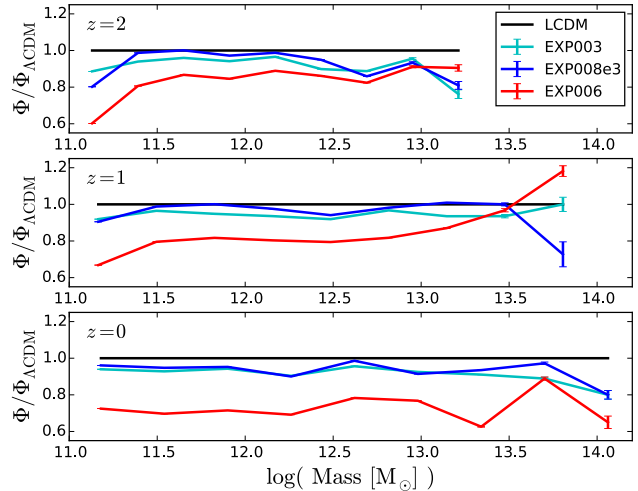


Figure 2. Ratio between the mass functions for the coupled dark energy cosmologies and the one from Λ CDM for redshifts $z = 2, 1, 0$ for the cosmological boxes of size 80 Mpc/h.

All the models share the same cosmological parameters and have at $z = 0$: $\Omega_{b0} = 0.0458$, $\Omega_{DM0} = 0.229$, $H_0 = 70.2$ km s $^{-1}$ Mpc $^{-1}$, $\sigma_8 = 0.816$, $n_s = 0.968$, where these parameters are density parameters for baryons and dark matter, Hubble constant, root mean square of the fluctuation amplitudes and primeval spectra index.

3.2 N-body Simulations

We first generate two sets of uniform particle distributions, a 80 Mpc/h box and a 12 Mpc/h box, both with 350^3 particles. The initial conditions were evolved with the code GADGET-2 (Springel 2005), which includes the coupled dark energy implementation introduced in Baldi et al. (2010). In Fig. 2 we show the ratio between the mass functions for the coupled dark energy cosmologies with the one from Λ CDM for redshifts $z = 2, 1, 0$ for our 80 Mpc/h boxes.

We chose four dark matter halos in the Λ CDM 80 Mpc/h box and one dwarf halo in the Λ CDM 12 Mpc/h box, and looked for their corresponding realizations in the coupled dark energy simulations. Note that we used the same random seed for all initial conditions to be able to follow the same halos in all cosmological boxes. Our halos have been chosen so that no other halos with comparable masses were found within four of their virial radii. We then re-ran the cosmological boxes with increased resolution in a Lagrangian volume that includes all particles that at $z = 0$ were found in three virial radii of each selected halo.

Our final sample is composed of three Milky-Way-size halos (halo α , halo β and halo γ), a $6 \times 10^{11} M_\odot$ halo (halo δ) and a dwarf halo (halo ϵ). For more details on the halos properties at $z = 0$ see Table 1. For the halo identification we used the code Amiga Halo Finder (Knollmann & Knebe 2009). The softening lengths are chosen to be $1/40$ of the intra-particle distance in the low resolution simulation divided by the refinement factor RF; RF = 15 for halo α , halo β and halo ϵ , RF = 24 for halo γ and halo δ . Precisely, the softening lengths are 0.54 kpc for halo α and halo β , 0.34 kpc for halo γ and halo δ , 0.081 kpc for halo ϵ . The particle masses at $z = 0$ in the high resolution volumes are

Table 1. Physical properties of the five halos in all cosmologies, Λ CDM, EXP003, EXP008e3 and EXP006. We show mass at R_{200} , R_{200} , concentrations and number of particles within R_{200} .

	M_{200} [M_\odot]	R_{200} [kpc]	$c \equiv R_{200}/r_s$	N_{200}
haloα				
Λ CDM	2.6×10^{12}	284	11.8	6.8×10^6
EXP003	2.5×10^{12}	281	9.1	6.6×10^6
EXP008e3	2.6×10^{12}	282	10.2	6.7×10^6
EXP006	2.1×10^{12}	265	4.6	5.5×10^6
haloβ				
Λ CDM	2.5×10^{12}	278	10.7	6.3×10^6
EXP003	2.2×10^{12}	267	8.0	5.7×10^6
EXP008e3	2.2×10^{12}	268	8.7	5.8×10^6
EXP006	1.7×10^{12}	246	4.3	4.5×10^6
haloγ				
Λ CDM	9.7×10^{11}	204	10.8	1.0×10^7
EXP003	9.3×10^{11}	201	8.6	9.9×10^6
EXP008e3	9.5×10^{11}	203	9.6	1.0×10^7
EXP006	7.6×10^{11}	188	3.2	8.1×10^6
haloδ				
Λ CDM	6.4×10^{11}	177	13.3	6.8×10^6
EXP003	5.6×10^{11}	170	9.7	6.0×10^6
EXP008e3	5.9×10^{11}	172	11.0	6.3×10^6
EXP006	5.3×10^{11}	166	4.7	5.6×10^6
haloϵ				
Λ CDM	4×10^9	33	15.3	3.1×10^6
EXP006	3×10^9	30	6.6	2.4×10^6

$3.8 \times 10^5 M_\odot$ for halo α and halo β , $9.4 \times 10^4 M_\odot$ for halo γ and halo δ , $1.3 \times 10^3 M_\odot$ for halo ϵ . In Fig. 3 we show the projected density maps of the four most massive halos for each cosmological model. We will discuss the dwarf halo in Section 4.3. For the density maps and throughout the paper we chose to calculate halo properties using R_{200} , radius at which the density is 200 times the critical density ρ_c , with $\rho_c \equiv 3H^2/(8\pi G)$.

4 RESULTS

4.1 Host Halos Properties

We first analyze the properties of the four most massive halos, halo α , halo β , halo γ and halo δ . We show concentrations, density profiles, rotation curves, evolution of the scale radius and accretion histories.

4.1.1 Concentrations and Density Profiles

By introducing a coupling between dark matter and dark energy, halo concentrations decrease. This was also shown in Baldi et al. 2010, Li & Barrow 2011, and Carlesi et al. 2014 for halos with masses $M \gtrsim 10^{13} M_\odot$. In this work we investigate mass scales $M \lesssim 10^{12} M_\odot$. The resolution that we are able to reach is higher thanks to the multi-mass technique. In Table 1 we show the concentration values for each halo, for which we use the definition

$$c \equiv R_{200}/r_s, \quad (6)$$

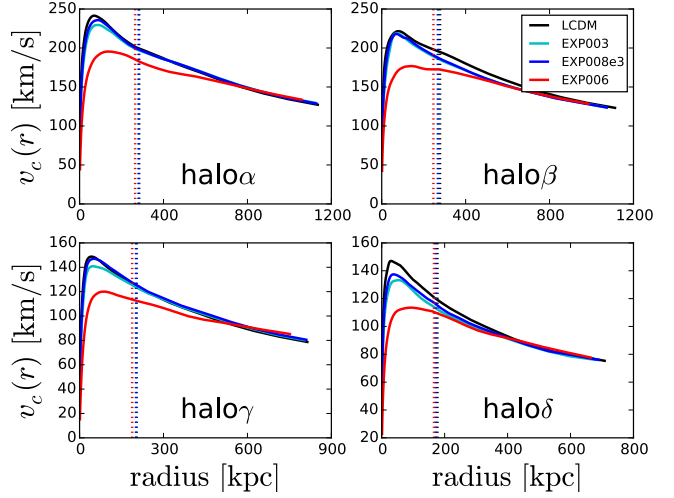


Figure 5. Rotation curves for halo α , halo β , halo γ and halo δ at $z = 0$, each for Λ CDM, EXP003, EXP008e3 and EXP006. The inner radius is equal to three times the softening length, while the outer radius is four times R_{200} of each halo. The vertical dashed lines mark R_{200} for each halo in each cosmology.

where R_{200} is the radius at which the density equals 200 times the critical density and r_s is the scale radius in the Navarro Frenk and White (NFW) profile (Navarro et al. 1997). We computed r_s via a χ^2 minimization procedure using the Levenberg & Marquart method as in Macciò et al. (2008). In agreement with literature, we find that halos which lived in a coupled dark energy cosmology have lower concentrations. Fig. 4 shows the density profiles for halo α , halo β , halo γ and halo δ . The behavior of the profiles as a function of cosmology is maintained for all four halos, with a significant flattening of the inner part of the profiles only for the extreme coupled cosmology EXP006, while differences are less evident in the EXP003 and EXP008e3 halos. Interestingly, the EXP006 realization of halo γ ($M = 7.6 \times 10^{11} M_\odot$) produces a much flatter halo profile, with slope $\alpha = -0.8$, which falls out of NFW parametrization. On the other hand, all other profiles of halo α , halo β , halo γ and halo δ in all cosmologies are well described by the NFW profile.

Additionally, in Fig. 5 we show the rotation curves at $z = 0$ for the four halos. For models within the observational constraints the rotation curves are not significantly affected. The only case in which we observe a considerable flattening is the extreme model EXP006, for all four cases. This is in agreement with Penzo et al. (2014), where we find that differences in rotation curves among models within observational constraints for dynamical dark energy are not significant in the dark matter only case. On the contrary, in hydrodynamical simulations we find observable differences in rotation curves due to the effects of baryons which enhance the variations in the dark matter accretion. We expect the same enhancement also in coupled dark energy models once hydrodynamics is taken into account. This aspect will be explored in a future work.

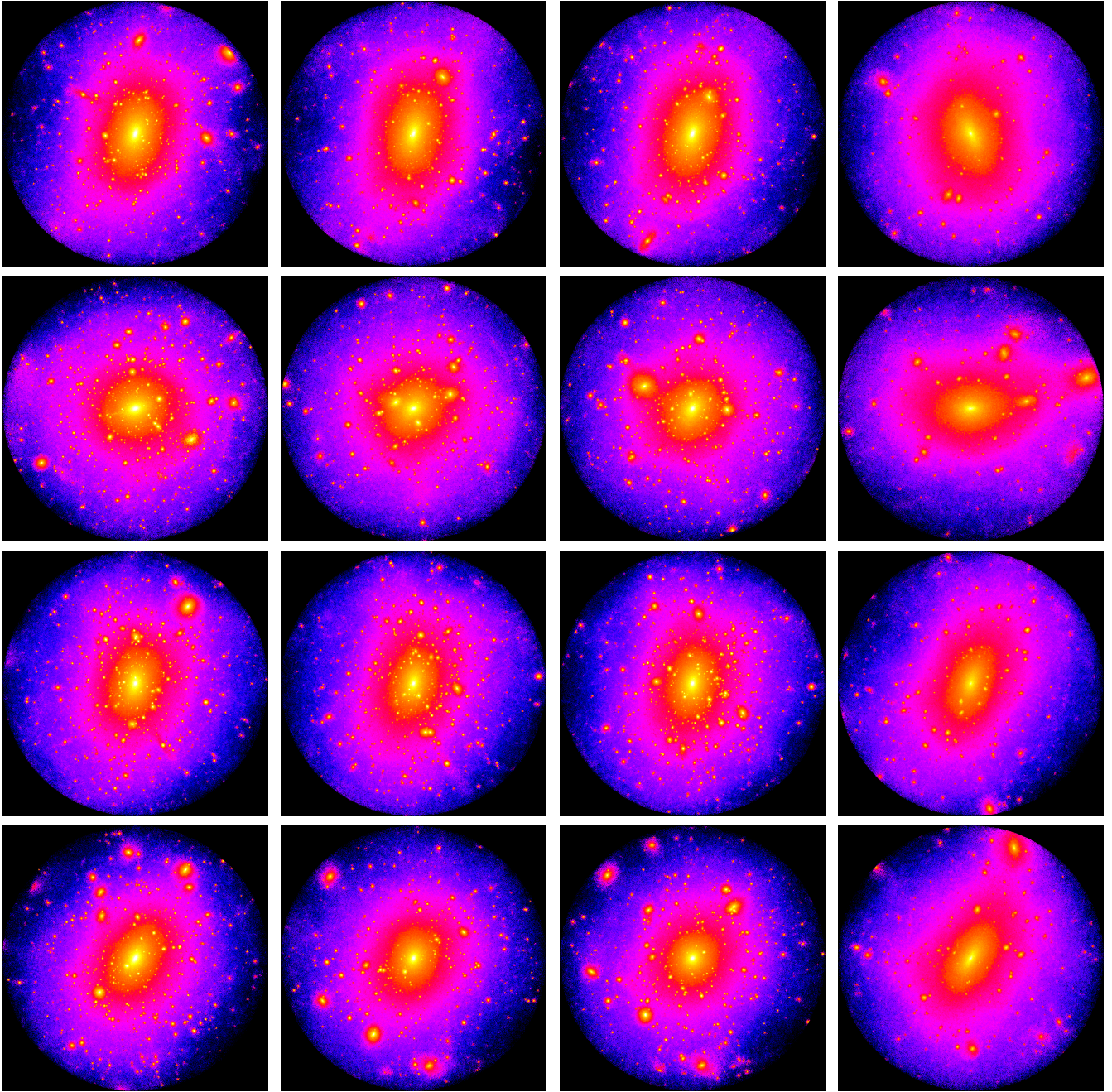


Figure 3. Projected density maps of our sample at $z = 0$. From first row to last we are showing halo α , halo β , halo γ , halo δ ; from first column to last we are showing Λ CDM, EXP003, EXP008e3 and EXP006 cosmologies. All images are spheres of radius R_{200} , radius at which the density is equal to 200 times the critical density.

4.1.2 NFW Scale Radius Evolution

In the Section 4.1.1 we have showed that halos that form in a coupled dark energy cosmology with a high value for the coupling constant have concentrations that are significantly lower at $z = 0$. Given that almost all halos are well described by a NFW density profile, it means that their NFW scale radii r_s are much larger than the scale radii of the corresponding Λ CDM realizations. In Fig. 6 we show the behavior of the scale radius r_s as a function of redshift for halo β in all four cosmologies; the other Milky-Way size

halos have similar behaviors. Compared to the Λ CDM case, halos which live in coupled dark energy cosmologies show a larger scale radius at all redshifts.

4.1.3 Main Halos Accretion Histories

In order to investigate the origin of the different concentrations, especially in the EXP006 cosmology, in this Section we concentrate on the halo formation times. Firstly, in Fig. 7 we show the accretion histories, namely the evolution of the mass enclosed in R_{200} normalized to the value of the mass

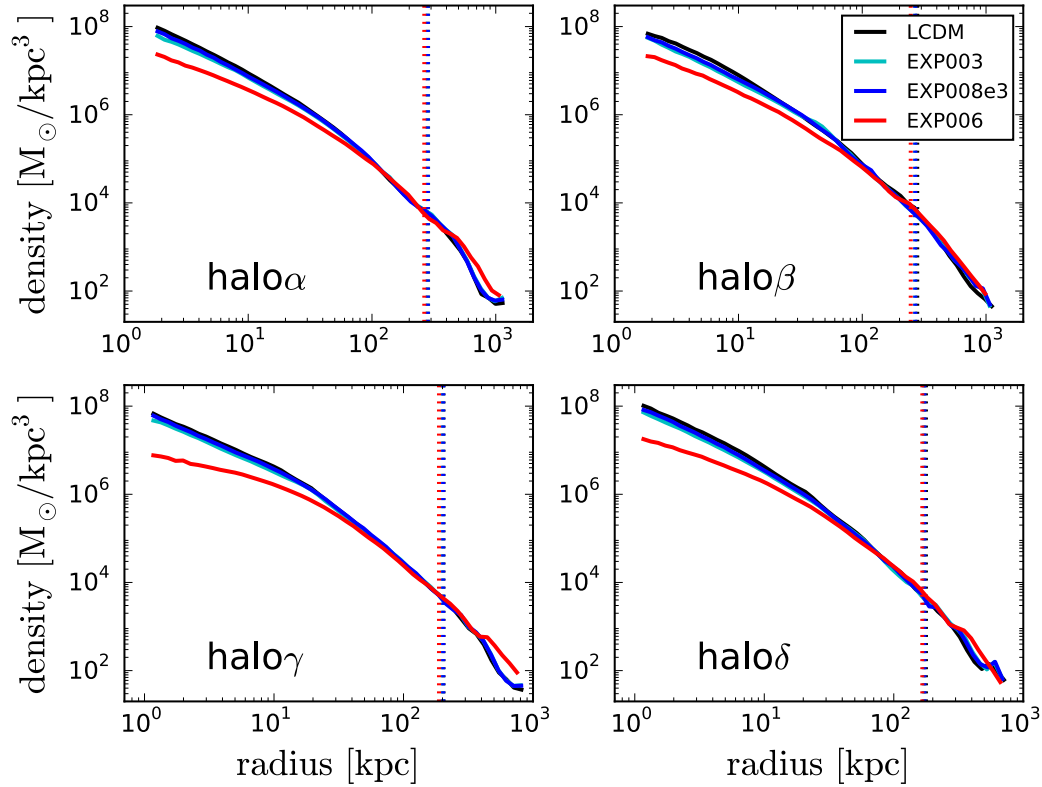


Figure 4. Density profiles for halo α , halo β , halo γ and halo δ at $z = 0$, each for Λ CDM (black), EXP003 (cyan), EXP008e3 (blue) and EXP006 (red). The inner radius is equal to three times the softening length, while the outer radius is four times R_{200} of each halo. The vertical dashed lines mark R_{200} for each halo in each cosmology.

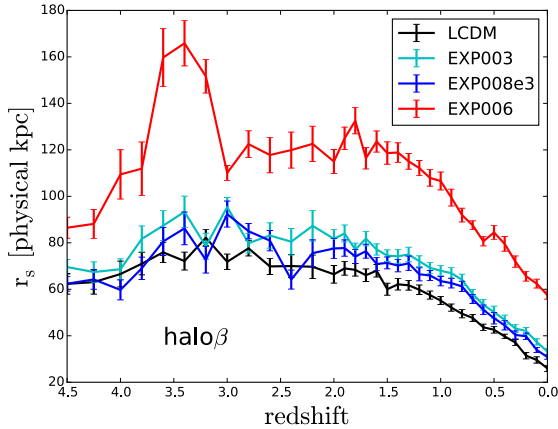


Figure 6. Scale radius obtained by fitting an NFW density profile using the Levenberg & Marquart method for halo β as a function of redshift.

at $z = 0$ as a function of expansion factor $a = 1/(1+z)$. Halos growing in Λ CDM, EXP003 and EXP008e3 cosmologies show similar accretion histories especially for halo α and halo γ ; while halos living in the EXP006 cosmology accrete their mass earlier on compared to their Λ CDM realizations. Among the three halos, coupled cosmologies runs show unexpected drops in the accretion histories. These would be unusual in a Λ CDM scenario since halo total masses do not decrease unless it is a temporary effect of a merger (see for instance halo α and halo β around $a = 0.3$). On the other

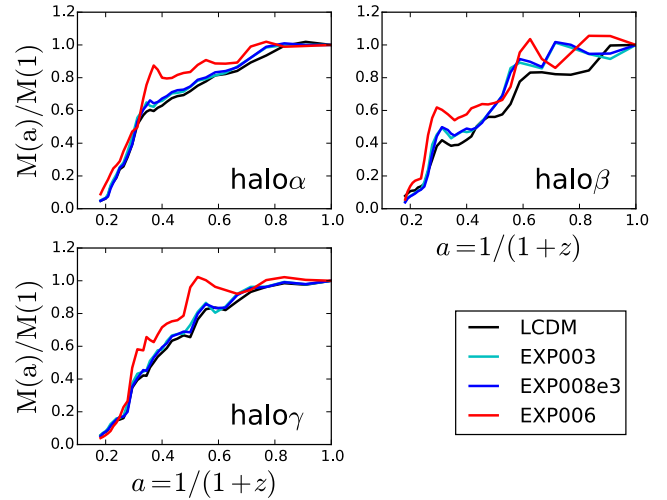


Figure 7. Evolution of the mass enclosed in R_{200} normalized to the mass at $a = 1$ as a function of the scale factor for halo α , halo β , halo γ in all four cosmologies.

hand, in the case of coupled cosmologies the friction term in Eq. 4 is responsible for injecting kinetic energy into the system, which may cause some particles to become gravitationally unbound.

In order to estimate the time of formation for each halo, we followed the approach described in Wechsler et al. (2002). In their paper they show how halo accretion histories are

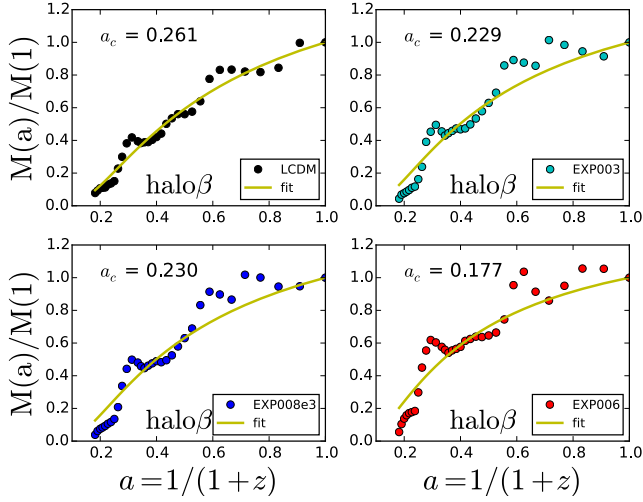


Figure 8. Accretion histories for halo β , where we show for each panel a different cosmological model. The fit to the accretion histories of each realization (solid yellow line) is obtained from Eq. 7.

Table 2. Values for the formation epochs a_c for halo α , halo β , halo γ in all four cosmologies.

	Λ CDM	EXP003	EXP008e3	EXP006
halo α	0.194	0.181	0.183	0.142
halo β	0.261	0.229	0.230	0.177
halo γ	0.225	0.210	0.215	0.173

well described by an exponential form that depends on one parameter, the formation epoch a_c , which is defined as the expansion factor at which the logarithmic derivative of the mass evolution falls below a critical value S . Specifically, the fitting form is given by

$$\frac{M(a)}{M(1)} = \exp \left[-a_c S \left(\frac{1}{a} - 1 \right) \right] \quad (7)$$

with $S = 2$. We used the fitting function of Eq. 7 to compute the formation epochs for each of the three halos for all cosmologies. As an example, we show in Fig. 8 the fitting result for halo β and we summarize the formation epochs for all halos in Table 2.

As pointed out in Wechsler et al. (2002), Dutton & Macciò (2014) and Ludlow et al. (2013), in a Λ CDM cosmology an early formation epoch leads to higher concentrations. The same happens for dynamical dark energy cosmologies, e.g. Klypin et al. (2003); Dolag et al. (2004). Interestingly, in coupled dark energy cosmology this behavior is not preserved. Despite the fact that a stronger coupling brings to an earlier halo formation epoch, halo concentrations decrease when the coupling is increased, as clearly visible from the EXP006 realizations. This phenomenon has also been showed in Baldi et al. (2010) and Baldi (2011), where an analysis of the modifications due to the coupling has been extensively carried out. The result is that the friction term in Eq. 4 is responsible for making the halo expand by altering its virial equilibrium through the injection of kinetic energy in the system, which in turns lowers the concentration (see Baldi 2011). This shows how in coupled

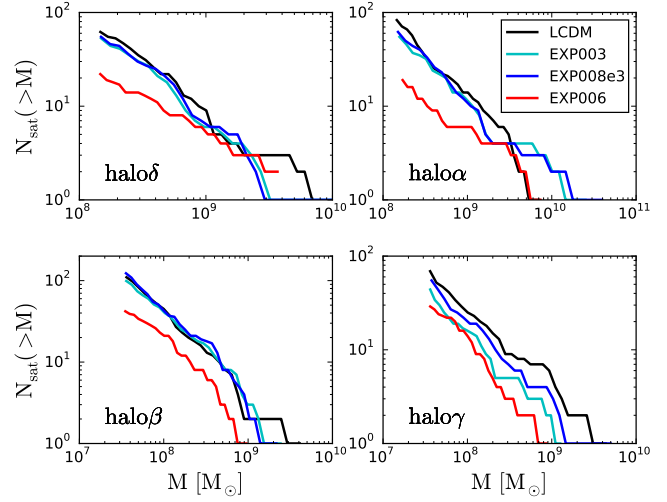


Figure 9. Cumulative number of subhalos with more than 400 particles as function of their mass for halo α , halo β , halo γ and halo δ at $z = 0$ for each cosmology.

cosmologies the lower concentrations are not the result of formation histories but the effect of the modified dynamics.

4.2 Subhalos

In this Section we study the subhalo abundance, their radial distribution and circular velocities.

4.2.1 Abundance

The lower number of substructures present in EXP006 halos compared to Λ CDM can be recognized in Fig. 3. In Fig. 9 we show the subhalo mass function, where only subhalos that lie within R_{200} and that have more than 400 particles are considered. The total number of subhalos in EXP006 realizations is always from 50 to 75% lower than in the respective Λ CDM cases, while differences between EXP003 and EXP008e3 and Λ CDM are much less evident ($\sim 10\%$). Thus, the missing satellites problem (Klypin et al. 1999; Moore et al. 1999) can be progressively alleviated when increasing the coupling. Note that the differences in the subhalos minimum mass among halo α , halo β and halo γ , halo δ are due to the different resolutions used (see Section 3.2).

4.2.2 Radial Distribution

Fig. 10 shows the cumulative distribution of subhalos as a function of the distance from the main halo center normalized to the total number of subhalos within R_{200} . All halos in all cosmologies show non-significant differences in the cumulative radial distribution. In order to better understand the distribution of subhalos, in Fig. 11 we show the differential distribution in a sphere of constant radius for all cosmologies, the radii are 350 kpc for halo α and halo β , 250 kpc for halo γ and 200 kpc halo δ . The number of bins is kept the same for each halo in all cosmologies and the vertical lines show the virial radii. The distributions show a clear

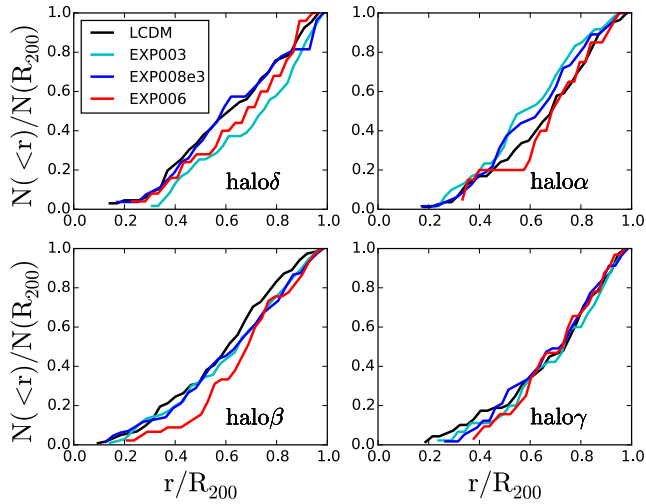


Figure 10. Cumulative number of subhalos with more than 400 particles as function of distance from the main halo center for halo α , halo β , halo γ and halo δ at $z = 0$ for each cosmology.

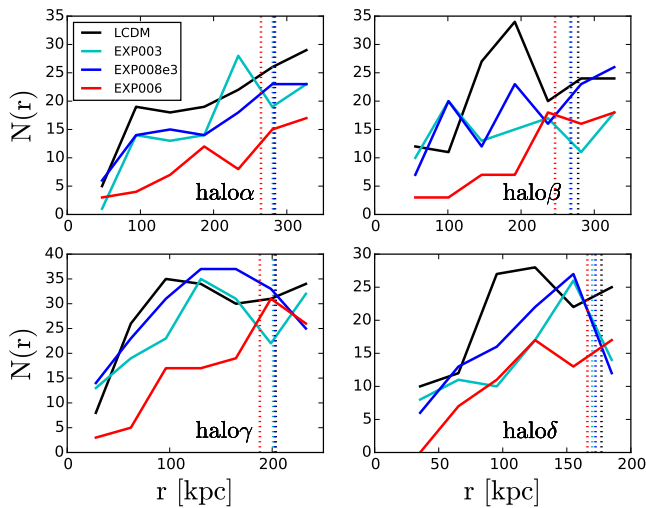


Figure 11. Differential number of subhalos in R_{200} with more than 400 particles as function of distance from main halo center for halo α , halo β , halo γ and halo δ at $z = 0$ for each cosmology. The vertical dashed lines mark R_{200} for each halo in each cosmology. For a given halo, the binning is kept constant for all cosmologies.

decrease of the number of subhalos in EXP006 halos compared to their respective Λ CDM cases, while for EXP003 and EXP008e3 cosmologies differences are not so evident.

As pointed out in Section 4.1.3, coupled cosmologies decrease halo concentrations thanks to the presence of a friction term in the equation for the evolution of density perturbations (Eq. 4), despite the earlier halo formation epochs. We claim that the same effect can be responsible for the lower number of subhalos compared to Λ CDM. Thanks to the extra friction term and to subhalo lower concentrations, subhalos that are falling into the main halo potential well are more heavily stripped, thus less halos with more than 400 particles survive. If this claim is correct, we should be able to find a difference in the subhalos number distribution when we reach distances from the main halo center that are bigger than the radius from which the gravitational influence of the

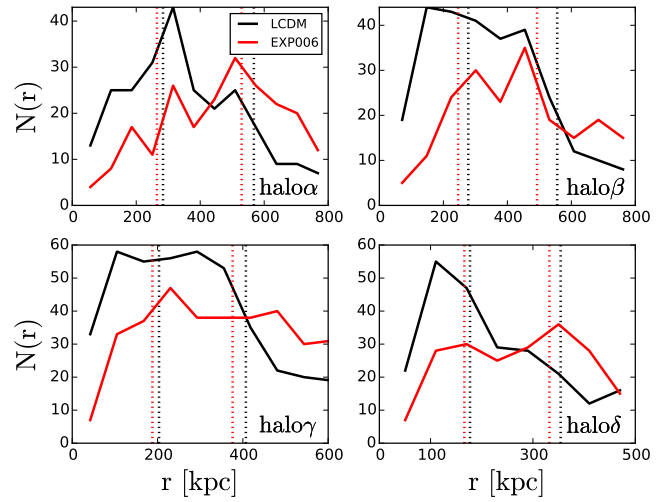


Figure 12. Number of subhalos in $3R_{200}$ with more than 400 particles as function of distance from main halo center for halo α , halo β , halo γ and halo δ at $z = 0$ for each cosmology. The vertical dashed lines mark R_{200} and $2R_{200}$ for each halo in each cosmology. For a given halo, the binning is kept constant for all cosmologies.

host halo is felt. In Fig. 12 we show the differential radial distribution of the number of subhalos out to about three times the virial radius of each halo. For the sake of clarity, we choose to show only the most extreme cases, EXP006, and Λ CDM for all four halos. The dotted lines represent one and two times R_{200} for each halo in each cosmology. What we would like to stress, is that there seem to be a decrease in the number of subhalos in halos living in EXP006 cosmology compared to their Λ CDM realizations *only* within the gravitational influence of the main halo. Between 1.5 and 2 R_{200} this behavior inverts and halos living in the strongly coupled cosmology seem to have a larger or at least a comparable number of subhalos with respect to their Λ CDM cases. Thus, we ascribe the presence of a lower subhalos number to a massive stripping effect rather than EXP006 producing intrinsically a lower number of subhalos. We would like to stress on the fact that lowering the number of subhalos can also be achieved by warm dark matter cosmologies (e.g. [Anderson et al. 2013](#)), but the fundamental difference lies on the fact that those subhalos in warm dark matter cosmologies were never formed, while in coupled dark energy cosmologies subhalos do form but they are heavily stripped.

4.2.3 Circular Velocities

[Boylan-Kolchin et al. \(2011\)](#) first showed that N-body simulations of a Milky-Way size halo predict a significant number of subhalos with circular velocities higher than the circular velocities that we measure for the brightest satellites of the Milky Way, which is surprising since these massive subhalos should not fail in producing stars.

The discrepancy between Λ CDM prediction and observations can be alleviated in multiple ways, starting from baryonic processes. [Brooks & Zolotov \(2014\)](#) suggest that baryonic feedback processes could be responsible for a dark matter redistribution, with the result of decreasing the central densities of the most massive subhalos. [Rashkov et al.](#)

(2012) point out that the possibility of star formation being stochastic below a certain mass would justify the Milky Way having massive dark satellites; furthermore, they highlight the fact that the tension between the Via Lactea II simulation and observations is only a factor of two in mass, which suggests that the uncertainty on the Milky Way virial mass could be a viable way out from the tension (Vera-Ciro et al. 2013; Kennedy et al. 2014). Purcell & Zentner (2012) showed that there exists a significant variation in subhalo properties even when the host halos have the same virial mass.

Last but not least, the discrepancy can be alleviated by appealing to non- Λ CDM cosmologies. The cases for warm, mixed (cold and warm) and self-interacting dark matter are considered respectively in Lovell et al. (2012), Anderhalden et al. (2012, 2013), Vogelsberger et al. (2012). In all cases they find that subhalos are less concentrated due to their late formation time, suggesting that alternative cosmologies can contribute to alleviate the tension between predictions and observations.

In Fig. 13 we show the rotation curves for the twelve most massive subhalos at the moment of infall. We used the correlation between orbital energy and subhalo mass loss found in Anderhalden et al. (2013) to determine the subhalos ranking. Each row illustrates the twelve subhalos rotation curves for a given main halo in all considered cosmologies, from the top down we show halo α , halo β , halo γ , halo δ . In yellow we show the observed values for $v_{\text{circ}}(r_{1/2})$ for the brightest dwarf galaxies orbiting around the Milky Way, data are taken from Anderhalden et al. (2013) and references therein. Despite halo α and halo β having comparable masses, the tension between simulated curves and measured points in the Λ CDM case is more evident in halo β , supporting the fact that subhalo properties can vary even when host halos have the same virial mass (Purcell & Zentner 2012). The tension is alleviated in the case of halo γ and even more halo δ , given their lower masses (Vera-Ciro et al. 2013). Overall, when looking at all halos in EXP003 and EXP008e3 cosmologies these do not show significant improvement compared to their Λ CDM realizations in decreasing the inner densities of subhalos. On the other hand, in the case of EXP006 cosmology, all four halos show such a dramatic decrease in subhalos rotational velocity peaks that rotation curves become incompatible with measured values. The dramatic decrease was to be expected given the choice of a large coupling parameter for EXP006 cosmology, but nonetheless it is useful to understand the effects of the coupling.

4.3 Zooming-in on a dwarf halo

To better explore the effects of the coupling at high resolutions, we simulated a dwarf galaxy halo, halo ϵ . We chose an isolated halo (no structures with comparable mass within four of its virial radii) and, given the results of Section 4.2, we only focused on the two most distant cosmological cases, Λ CDM and EXP006 cosmology. The virial masses are respectively $4 \times 10^9 M_\odot$ and $3 \times 10^9 M_\odot$, with a mass resolution of $1.3 \times 10^3 M_\odot$. We show in Fig. 14 the density maps for halo ϵ in both cosmologies, Λ CDM on the upper panel. It is visible how the number of substructures decreases in the case with coupling. In Fig. 15 we show density profiles and rotation curves for halo ϵ in both cosmologies. The effect of the

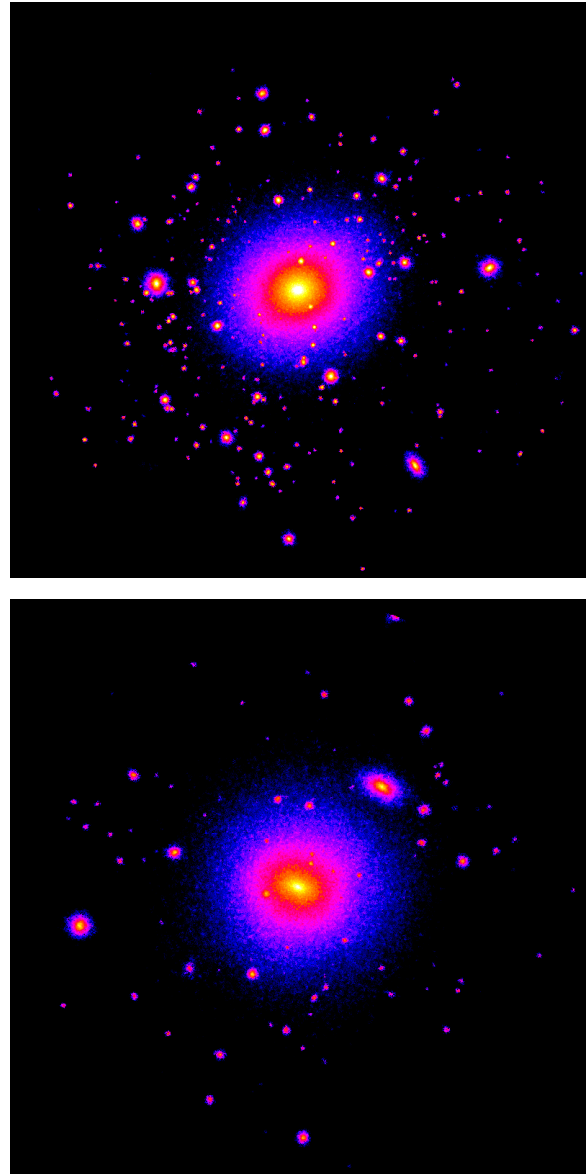


Figure 14. Density maps for halo ϵ in Λ CDM (upper panel) and in EXP006 cosmology (lower panel). The side of each projection is $2 \times R_{200}$.

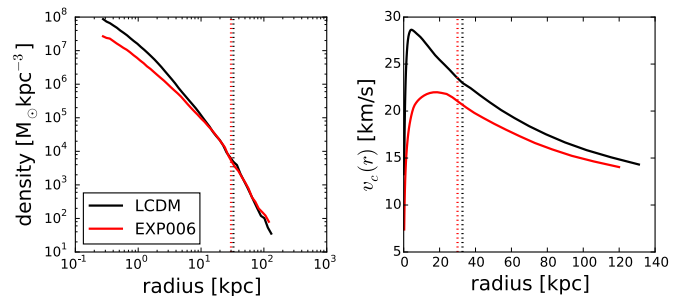


Figure 15. Density profiles and rotation curves for halo ϵ in Λ CDM (black) and in EXP006 (red) cosmology. The inner minimum radius is three times the softening length, while the most outer radius is four times R_{200} respectively. The vertical dashed lines represent R_{200} for each cosmology.

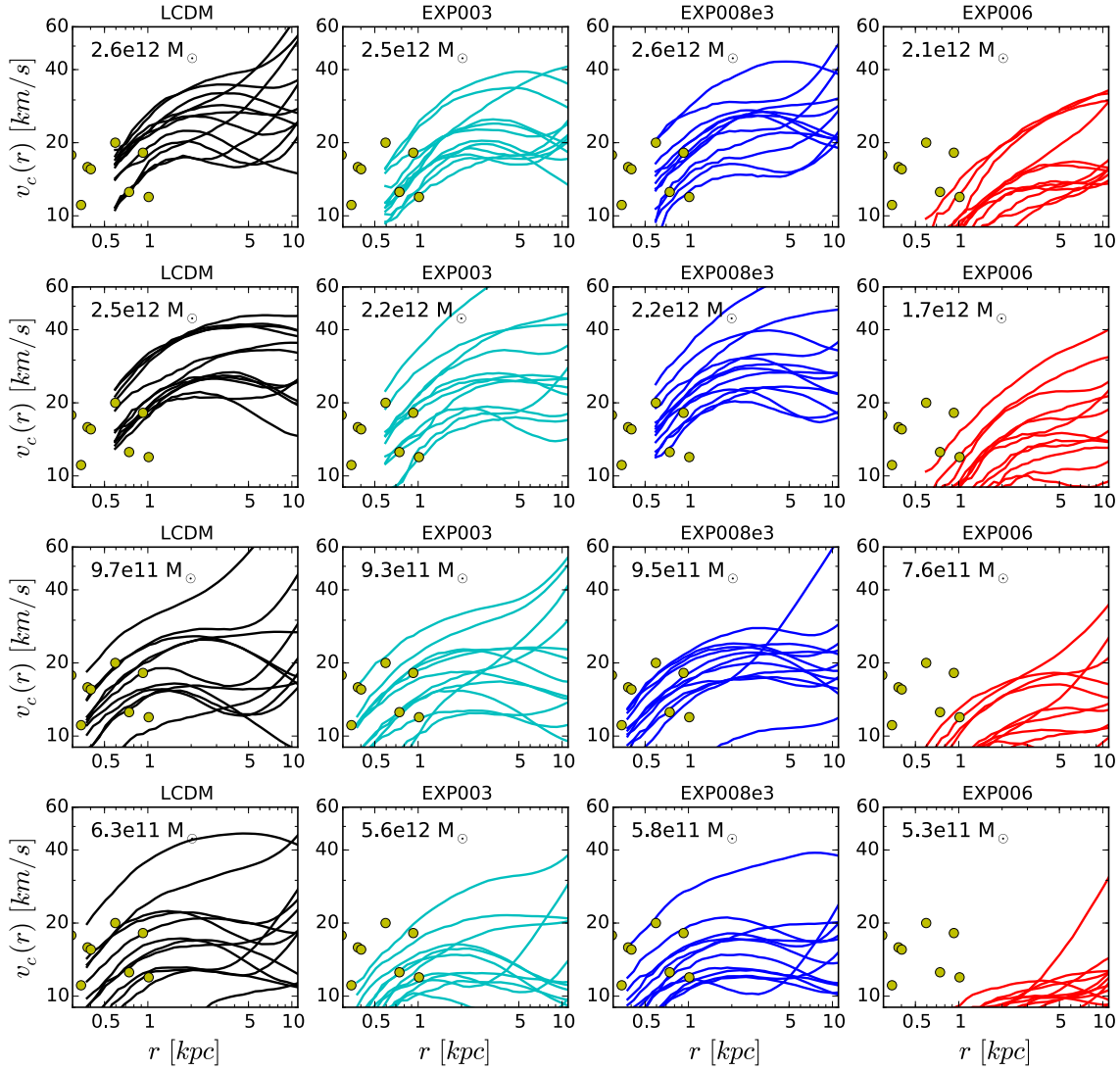


Figure 13. Rotation curves of the most massive subhalos at the moment of infall for each halo in each cosmology. From the top row down we show halo α , halo β , halo γ , halo δ , from left to right we show Λ CDM (black), EXP003 (cyan), EXP008e3 (blues), EXP006 (red). We estimate the subhalo mass ranking at the moment of infall using the correlation between orbital energy and subhalo mass loss found in [Anderhalden et al. \(2013\)](#). The yellow points are the observed values for $v_{\text{circ}}(r_{1/2})$ for the brightest dwarf galaxies orbiting around the Milky Way. Data are taken from [Anderhalden et al. \(2013\)](#) and references therein. The masses of each main halo realizations is written on each panel.

coupling is very evident in lowering the concentration and flattening the rotation curve. The values for the halo concentrations are $c = 15.2$ and $c = 6.5$ for Λ CDM and EXP006 cosmology respectively. Although the density profile in the coupled dark energy case is less concentrated, it is still cuspy, showing that in coupled cosmologies, as in Λ CDM, we are not able to produce a dark matter only cored density profile. The inconsistency with observation thus still persists, given the observational evidence that supports cored density profiles for the satellites of the Milky Way ([Walker & Peñarrubia 2011](#); [Amorisco & Evans 2012](#); [Amorisco et al. 2013](#)). Interesting to note, by constructing a model in which both warm and cold dark matter are present and only the cold component is coupled to dark energy, a very high value ($\beta_c \sim 10$) for the coupling constant is favored ([Bonometto](#)

[et al. 2015](#)) and simulated dark matter only dwarf halos show a cored density profile ([Macciò et al. 2015](#)). Fig. 16 shows accretion histories, the ratio of M_{200} to its value today is plotted as function of scale factor. As in Section 4.1.3, we calculated the formation epochs as in [Wechsler et al. \(2002\)](#) and obtained $a_c = 0.191$ (Λ CDM), $a_c = 0.146$ (EXP006), confirming the finding that coupled dark energy models have earlier formation times, also for less massive halos.

5 CONCLUSIONS

We have performed the first study in coupled dark energy cosmologies on high resolution simulations on galactic scales, with the aim to study the effects of the coupling between dark energy and dark matter on these scales, so

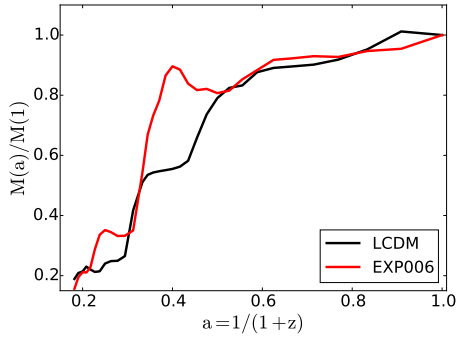


Figure 16. Accretion histories for haloes in Λ CDM (black) and in EXP006 (red) cosmology. We show the ratio of M_{200} at a given time and M_{200} today as a function of the scale factor.

far neglected in previous studies. We chose to investigate two viable models, one with constant coupling and one with varying coupling with redshift; we also chose a third case where the constant coupling value has been pushed beyond observational constraints to better investigate its effects. We then selected three Milky-Way size halos, a $6 \times 10^{11} M_{\odot}$ halo and a dwarf halo $5 \times 10^9 M_{\odot}$, and studied their properties in a Λ CDM reference model and in the coupled cosmologies, resolving each halo with $\sim 10^6$ particles.

We computed concentrations and formation epochs for all halos and we find that, despite the earlier formation epochs of the coupled cosmologies halos, these have lower concentrations. In a Λ CDM or a dynamical dark energy scenario, earlier formation epochs would imply higher concentrations, but in the coupled dark energy case the reason for lower concentrations is not related to formation histories, but rather to the modified dynamics. In fact, the equation for the linear evolution of density perturbations (Eq. 4) shows the friction term $-\beta\dot{\phi}\dot{\delta}_c$, an extra term compared to the Λ CDM case that redistributes the dark matter particles and lowers the central densities, despite the earlier formation times (see Baldi 2011). We find that this behavior is reproduced for all mass scales that we have investigated.

In particular, subhalos can also be significantly less concentrated. When falling towards their host, they are more heavily stripped once they start feeling the gravitational influence of the host halo. This translates into decreasing the number of subhalos compared to the Λ CDM realization and, additionally, subhalos are themselves less massive and less concentrated. For these reasons, coupled cosmologies can be helpful in alleviating satellite-scales inconsistencies of Λ CDM. On the other hand, we find that in order to try to solve these issues with the coupling alone, one needs to use an extreme value for the coupling constant that is ruled out by observational constraints. In fact, only in the case with the highest coupling value the number of subhalos is significantly reduced (up to 75% less subhalos) than in the respective Λ CDM cases, while for the viable coupling cosmologies the decrease is much less significant (10% less subhalos). Moreover, we find that the distribution of the subhalos inside the main halo virial radius does not vary significantly among cosmologies. Lastly, less concentrated coupled cosmologies subhalos can in principle be useful to reconcile the inconsistency between the observed properties of the Milky Way dwarf galaxies and Λ CDM simulations pre-

dictions, but once more a high enough value for the coupling must be assumed. Interestingly, allowing the introduction of massive neutrinos does alleviate the constraints on the coupling (see e.g. La Vacca et al. 2009), leaving coupled dark energy models dynamics on sub-galactic scales an interesting option.

Overall coupled dark energy models can be as effective as Λ CDM in reproducing observations on sub-galactic scales and, for specific choices of the coupling, they can improve the agreement between predicted and observed properties. Hence, coupled models would need to be further investigated, possibly taking into account the effects of baryons at sub-galactic scales, which, as already shown in dynamical dark energy models (Penzo et al. 2014), are expected to amplify differences observed in the dark matter only case.

ACKNOWLEDGMENTS

The numerical simulations were performed on the THEO cluster of the Max-Planck-Institut für Astronomie and Hydra cluster, both based at the Rechenzentrum in Garching. CP and AVM acknowledge the support from the Sonderforschungsbereich SFB 881 The Milky Way System (subproject A02) of the German Research Foundation (DFG). CP also acknowledges the support of the International Max Planck Research School, Heidelberg (IMPRS-HD). MB acknowledges partial support by the Marie Curie Intra European Fellowship “SIDUN” within the 7th Framework Programme of the European Commission. LC acknowledges the Brazilian research Institutions FAPES and CNPq for financial support.

REFERENCES

- Agnello, A., & Evans, N. W. 2012, *ApJL*, 754, L39
- Alam, S., Albareti, F. D., Allende Prieto, C., et al. 2015, *ArXiv e-prints*, arXiv:1501.00963
- Amendola, L. 2000, *Phys. Rev. D*, 62, 043511
- . 2004, *Phys. Rev. D*, 69, 103524
- Amendola, L., Gasperini, M., & Piazza, F. 2004, *Journal of Cosmology and Astroparticle Physics*, 9, 14
- Amendola, L., & Tocchini-Valentini, D. 2001, *Phy.Rev.D*, 64, 043509
- Amorisco, N. C., Agnello, A., & Evans, N. W. 2013, *MNRAS*, 429, L89
- Amorisco, N. C., & Evans, N. W. 2012, *MNRAS*, 419, 184
- Anderhalden, D., Diemand, J., Bertone, G., Macciò, A. V., & Schneider, A. 2012, *Journal of Cosmology and Astroparticle Physics*, 10, 47
- Anderhalden, D., Schneider, A., Macciò, A. V., Diemand, J., & Bertone, G. 2013, *Journal of Cosmology and Astroparticle Physics*, 3, 14
- Anderson, G. W., & Carroll, S. M. 1998, in *COSMO-97, First International Workshop on Particle Physics and the Early Universe*, ed. L. Roszkowski, 227
- Baldi, M. 2011, *MNRAS*, 414, 116
- . 2012, *MNRAS*, 422, 1028
- Baldi, M., Pettorino, V., Robbers, G., & Springel, V. 2010, *MNRAS*, 403, 1684
- Bertschinger, E. 2001, *ApJS*, 137, 1

- Billyard, A. P., & Coley, A. A. 2000, *Phy.Rev.D*, 61, 083503
- Bonometto, S. A., Mainini, R., & Macciò, A. V. 2015, ArXiv e-prints, arXiv:1503.07875
- Boylan-Kolchin, M., Bullock, J. S., & Kaplinghat, M. 2011, *MNRAS*, 415, L40
- Brooks, A. M., & Zolotov, A. 2014, *ApJ*, 786, 87
- Carlesi, E., Knebe, A., Lewis, G. F., Wales, S., & Yepes, G. 2014, *MNRAS*, 439, 2943
- Di Cintio, A., Brook, C. B., Macciò, A. V., et al. 2014, *MNRAS*, 437, 415
- Diemand, J., Zemp, M., Moore, B., Stadel, J., & Carollo, C. M. 2005, *MNRAS*, 364, 665
- Dolag, K., Bartelmann, M., Perrotta, F., et al. 2004, *Astronomy and Astrophysics*, 416, 853
- Dutton, A. A., & Macciò, A. V. 2014, *MNRAS*, 441, 3359
- Farrar, G. R., & Peebles, P. J. E. 2004, *ApJ*, 604, 1
- Flores, R. A., & Primack, J. R. 1994, *ApJL*, 427, L1
- Gentile, G., Famaey, B., Zhao, H., & Salucci, P. 2009, *Nature*, 461, 627
- Governato, F., Zolotov, A., Pontzen, A., et al. 2012, *MNRAS*, 422, 1231
- Gromov, A., Baryshev, Y., & Teerikorpi, P. 2004, *Astronomy and Astrophysics*, 415, 813
- Guo, Z.-K., Ohta, N., & Tsujikawa, S. 2007, *Phy.Rev.D*, 76, 023508
- Jones, D. H., Read, M. A., Saunders, W., et al. 2009, *MNRAS*, 399, 683
- Kennedy, R., Frenk, C., Cole, S., & Benson, A. 2014, *MNRAS*, 442, 2487
- Klypin, A., Kravtsov, A. V., Valenzuela, O., & Prada, F. 1999, *ApJ*, 522, 82
- Klypin, A., Macciò, A. V., Mainini, R., & Bonometto, S. A. 2003, *ApJ*, 599, 31
- Knollmann, S. R., & Knebe, A. 2009, *ApJS*, 182, 608
- Koivisto, T. 2005, *Phy.Rev.D*, 72, 043516
- La Vacca, G., Kristiansen, J. R., Colombo, L. P. L., Mainini, R., & Bonometto, S. A. 2009, *JCAP*, 0904, 007
- Lewis, A., & Bridle, S. 2002, *Phys. Rev.*, D66, 103511
- Li, B., & Barrow, J. D. 2011, *Phys. Rev.*, D83, 024007
- Lovell, M. R., Eke, V., Frenk, C. S., et al. 2012, *MNRAS*, 420, 2318
- Ludlow, A. D., Navarro, J. F., Boylan-Kolchin, M., et al. 2013, *MNRAS*, 432, 1103
- Macciò, A. V., Dutton, A. A., & van den Bosch, F. C. 2008, *MNRAS*, 391, 1940
- Macciò, A. V., Kang, X., Fontanot, F., et al. 2010, *MNRAS*, 402, 1995
- Macciò, A. V., Mainini, R., Penzo, C., & Bonometto, S. A. 2015, ArXiv e-prints, arXiv:1503.07867
- Macciò, A. V., Quercellini, C., Mainini, R., Amendola, L., & Bonometto, S. A. 2004, *Phy.Rev.D*, 69, 123516
- Madau, P., Diemand, J., & Kuhlen, M. 2008, *ApJ*, 679, 1260
- Mangano, G., Miele, G., & Pettorino, V. 2003, *Modern Physics Letters A*, 18, 831
- Matarrese, S., Pietroni, M., & Schimd, C. 2003, *Journal of Cosmology and Astroparticle Physics*, 8, 5
- Moore, B. 1994, *Nature*, 370, 629
- Moore, B., Ghigna, S., Governato, F., et al. 1999, *ApJL*, 524, L19
- Navarro, J. F., Frenk, C. S., & White, S. D. M. 1997, *ApJ*, 490, 493
- Oñorbe, J., Boylan-Kolchin, M., Bullock, J. S., et al. 2015, ArXiv e-prints, arXiv:1502.02036
- Peebles, P. J. E., & Ratra, B. 1988, *ApJL*, 325, L17
- Penzo, C., Macciò, A. V., Casarini, L., Stinson, G. S., & Wadsley, J. 2014, *MNRAS*, 442, 176
- Perlmutter, S., Aldering, G., Goldhaber, G., et al. 1999, *ApJ*, 517, 565
- Pettorino, V., Amendola, L., Baccigalupi, C., & Quercellini, C. 2012, *Phy.Rev.D*, 86, 103507
- Planck Collaboration, Ade, P. A. R., Aghanim, N., et al. 2015, ArXiv e-prints, arXiv:1502.01589
- Purcell, C. W., & Zentner, A. R. 2012, *Journal of Cosmology and Astroparticle Physics*, 12, 7
- Rashkov, V., Madau, P., Kuhlen, M., & Diemand, J. 2012, *ApJ*, 745, 142
- Riess, A. G., Filippenko, A. V., Challis, P., et al. 1998, *The Astronomical Journal*, 116, 1009
- Salucci, P., Wilkinson, M. I., Walker, M. G., et al. 2012, *MNRAS*, 420, 2034
- Simon, J. D., Bolatto, A. D., Leroy, A., Blitz, L., & Gates, E. L. 2005, *ApJ*, 621, 757
- Springel, V. 2005, *MNRAS*, 364, 1105
- Swaters, R. A., Madore, B. F., van den Bosch, F. C., & Balcells, M. 2003, *ApJ*, 583, 732
- Tollerud, E. J., Beaton, R. L., Geha, M., et al. 2012, in *American Astronomical Society Meeting Abstracts*, Vol. 219, American Astronomical Society Meeting Abstracts 219, 201.04
- van den Bosch, F. C., & Swaters, R. A. 2001, *MNRAS*, 325, 1017
- Vera-Ciro, C. A., Helmi, A., Starkenburg, E., & Breddels, M. A. 2013, *MNRAS*, 428, 1696
- Vogelsberger, M., Zavala, J., & Loeb, A. 2012, *MNRAS*, 423, 3740
- Walker, M. G., & Peñarrubia, J. 2011, *ApJ*, 742, 20
- Wechsler, R. H., Bullock, J. S., Primack, J. R., Kravtsov, A. V., & Dekel, A. 2002, *ApJ*, 568, 52
- Weinberg, S. 1989, *Reviews of Modern Physics*, 61, 1
- Wetterich, C. 1988, *Nuclear Physics B*, 302, 668
- . 1995, *A & A*, 301, 321
- Zimdahl, W., Pavón, D., & Chimento, L. P. 2001, *Physics Letters B*, 521, 133

This paper has been typeset from a \LaTeX file prepared by the author.